JGR Atmospheres

RESEARCH ARTICLE
10.1029/2023JD040450

Polar Low Circulation Enhances Greenland's West Coast Cloud Surface Warming

Jean Lac[1], Hélène Chepfer[1], Assia Arouf[1], Matthew D. Shupe[2,3], and Michael R. Gallagher[2,3]

[1]LMD/IPSL, École Polytechnique, Institut Polytechnique de Paris, ENS, CNRS, PSL Université, Sorbonne Université, Palaiseau, France, [2]Cooperative Institute for Research in Environmental Sciences, University of Colorado, Boulder, CO, USA, [3]NOAA Physical Sciences Laboratory, Boulder, CO, USA

Key Points:

- The Greenland Ice Sheet (GrIS) west coast by itself represents 22% of the GrIS mass loss over the last two decades
- A polar low promotes the presence of low clouds over the GrIS west coast during the melt season
- The cloud surface radiative warming on the Greenland west coast is +10 W/m^2 larger in September than July due to these low clouds

Supporting Information:

Supporting Information may be found in the online version of this article.

Correspondence to:

J. Lac,
jean.lac@lmd.ipsl.fr

Citation:

Lac, J., Chepfer, H., Arouf, A., Shupe, M. D., & Gallagher, M. R. (2024). Polar low circulation enhances Greenland's west coast cloud surface warming. *Journal of Geophysical Research: Atmospheres*, *129*, e2023JD040450. https://doi.org/10.1029/2023JD040450

Received 23 NOV 2023
Accepted 14 MAY 2024

Author Contributions:

Data curation: Assia Arouf, Michael R. Gallagher
Formal analysis: Jean Lac
Funding acquisition: Hélène Chepfer
Investigation: Jean Lac, Hélène Chepfer, Assia Arouf, Matthew D. Shupe
Project administration: Hélène Chepfer
Resources: Assia Arouf, Michael R. Gallagher
Writing – original draft: Jean Lac
Writing – review & editing: Hélène Chepfer, Matthew D. Shupe

Abstract Mass loss of the Greenland Ice Sheet (GrIS) plays a major role in the global sea level rise. The west coast of the GrIS has contributed 1,000 Gt of the 4,488 Gt GrIS mass loss between 2002 and 2021, making it a hotspot for GrIS mass loss. Surface melting is driven by changes in the radiative budget at the surface, which are modulated by clouds. Previous works have shown the impact of North Atlantic transport for influencing cloudiness over the GrIS. Here we used space-based lidar cloud profile observations to show that a polar low circulation promotes the presence of low clouds over the GrIS west coast that warm radiatively the GrIS surface during the melt season. Polar low circulation transports moisture and low clouds from the sea to the west of Greenland up over the GrIS west coast through the melt season. The concomitance of the increasing presence of low cloud in fall over the Baffin Sea due to seasonal sea-ice retreat and a maximum occurrence of Polar low circulation in September results in a maximum of low cloud fraction (~14% at 2.5 km above sea level) over the GrIS west coast in September. These low clouds warm radiatively the GrIS west coast surface up to 80 W/m^2 locally. This warming contributes to an average increase of 10 W/m^2 of cloud surface warming in September compared to July on the GrIS west coast. Overall, this study suggests that regional atmospheric processes independent from North Atlantic transport may also influence the GrIS melt.

Plain Language Summary The melting of Greenland plays a major role in the global sea level rise. The west coast of Greenland has contributed to 22% of Greenland mass loss between 2002 and 2021, making it a hotspot for Greenland mass loss. Clouds modulate the energy that reaches the surface of Greenland and, therefore, might accelerate or decelerate surface melt. To explain what leads to cloud presence over Greenland, previous studies focused on the connection between the mid-latitudes and the Greenland cloud cover. Using a combination of satellite cloud observation and models, we highlight that a low-pressure system over the Arctic brings moisture and low clouds from the sea west of Greenland to the Greenland west coast. Then, we assess the strong surface warming effect of these low clouds. Overall, our study demonstrates that local Arctic processes lead to formation of low clouds where Greenland melts.

1. Introduction

Greenland contains the second largest ice sheet on Earth. In relation to global warming, its melting has accelerated to a loss of 280 Gt/year, corresponding to a contribution of 0.47 mm/year to sea level rise (Van den Broeke et al., 2016). The reliability of Greenland Ice Sheet (GrIS) melt prediction is important for predictions of the future Earth climate, as GrIS disappearance could lead to a global sea-level rise of 7 m (Bamber et al., 2013). Loss of Greenland ice mass occurs in the form of surface melting and ice discharge across the grounding line. Recent Greenland melt acceleration is mainly attributed to surface melting (Enderlin et al., 2014), which has reached a record over the last decades (Nghiem et al., 2012).

Melting of the ice sheet surface is driven by the surface energy budget, which is defined as the difference between the incoming and outgoing energy fluxes at the Greenland surface. This budget takes into account the radiative budget, as well as turbulent energy terms and changes in storage of heat within the ice-sheet. The radiative budget in the visible (shortwave) and thermal infrared (longwave) domains is modulated by the presence of clouds. Part of the longwave radiation emitted by the Greenland surface is absorbed by clouds and re-emitted downward to the surface, causing surface longwave warming relative to clear skies. By blocking the incoming solar shortwave radiation, clouds also produce a shortwave cooling at the surface. Due to the high albedo of the GrIS surface (0.8–0.95 at the Summit station, Miller et al., 2015), the shortwave cooling effect of clouds is weak over Greenland

compared to over open water. Thus, in contrast to other regions of the Earth with non icy surfaces, the longwave warming effect of clouds drives the total cloud radiative effect (shortwave cooling plus longwave warming) at the GrIS surface (C. Wang et al., 2019; W. Wang et al., 2019). However, this statement might be contradicted over the narrow coastal band where the GrIS surface albedo can be lower during the melt season (Hofer et al., 2017).

Amongst all cloud types, liquid-bearing clouds are known to play a critical role for surface melt, for instance during extreme melt events such as July 2012 (Bennartz et al., 2013), due to their high surface radiative warming effect produced by their relatively large optical depth compared to ice clouds (Shupe & Intrieri, 2004). They are observed mainly over the southeast and west coasts of the GrIS (Van Tricht et al., 2016). In order to understand the drivers of Greenland's cloud surface warming effect, it is necessary to understand the processes that lead to the presence of these liquid-bearing clouds. Analyzing large scale atmospheric circulations over Greenland, previous studies have shown that cyclonic conditions located in the Baffin Sea generally enhance the transport of cloudy airmasses from the North Atlantic to the GrIS coasts (Gallagher et al., 2020) whereas atmospheric blocking located above the GrIS typically block further transport, and thus decrease Greenland cloud cover (Hofer et al., 2017; Tedesco & Fettweis, 2020). In contrast to Greenland, the Arctic Ocean around the GrIS can also experience low cloud formation and low cloud dissipation via local processes, for example, atmosphere/ocean coupling in fall (Morrison et al., 2018) and sea-ice leads/atmosphere coupling in winter (Li et al., 2020). About cloud formation processes, newly open water due to the seasonal decrease of Arctic sea ice leads to an increase of low liquid-bearing clouds in the lowest 1 km above sea level during fall (Morrison et al., 2018).

Motivated by the need to understand drivers of the GrIS melt, we investigate the impact of low clouds in fall on the GrIS coasts. We first show (Section 3) that the GrIS west coast is responsible for the loss of a large portion of the overall GrIS mass loss over the last two decades. Then, to understand the GrIS west coast melt, we examine one process that can influence it, the cloud surface warming. In Section 4 we look for what conditions favor the occurrence of these low clouds during the melt season over the west GrIS coast. In Section 5 we analyze the increase of the surface radiative warming over the GrIS west coast due to low clouds during the melt season.

2. Data and Methods

2.1. Cloud Properties

CALIPSO-GOCCP cloud observations (Cesana & Chepfer, 2013; Chepfer et al., 2010; Guzman et al., 2017) from 2008 to 2020 are used in this study. These same observations have been used in previous polar studies (e.g., Cesana et al., 2012; Gallagher et al., 2020; Kay et al., 2008; Morrison et al., 2018) for their relevance over Arctic frozen surfaces (Lacour et al., 2017). Contrary to space-based passive sensors, these active sensor measurements are known to reliably observe clouds over all surface types. Although this product misses low thin ice clouds (ice water content <2.5 g/m^3), this is not a limitation for this study as the focus is on clouds with higher opacity that produce larger surface radiative effects and therefore drive the overall cloud impact on the Greenland surface radiative budget. We use CALIPSO-GOCCP at three different resolutions: (a) The monthly gridded ($1° \times 1°$) cloud fraction profile is used in Section 3.2. In each $1° \times 1°$ gridbox, the cloud fraction profile is defined as the sum of cloud detections at a given level of altitude, divided by the number of valid values at this same level of altitude. (b) The daily gridded ($1° \times 1°$) cloud fraction profile data set is used in Section 4 and 5 to describe processes that lead to low cloud presence over the GrIS west coast on a daily timescale. (c) The orbit data set with 480 m vertical resolution and horizontal resolutions of 90 m cross track and 330 m along track is used in Section 4.2 to get a better description of the cloud typology when low clouds occur over the GrIS west coast. Two orbits per day overfly the GrIS west coast, one orbit in the morning (between 4 and 6 a.m. LST) crosses the GrIS west coast and the Baffin Sea, and one orbit in the afternoon (between 12 and 2 p.m. LST) is parallel to the GrIS west coast (see CALIPSO orbit example Figure S4 in Supporting Information S1). We only use the morning subsample (4–6 a.m. LST) as it observes both the Baffin Sea and the GrIS west coast along each single orbit, which is useful to study the spatial cloud continuity between the two regions.

2.2. Surface Cloud Radiative Effect

The surface Cloud Radiative Effect (CRE) is used to quantify the radiative impact of clouds at the surface. The CRE is defined as the radiative downwelling fluxes at the surface over all types of scenes minus fluxes where the influence of clouds has been removed, in the visible domain (SWCRE) as well as in the longwave domain (LWCRE). Cloud detection by active sensors is more reliable than by passive sensors above highly reflective

surfaces such as frozen ice or snow. As highlighted by Arouf et al. (2022), although not seeing the cloud base height induces some biases, estimation of surface LWCRE based on active sensors remains the best option while comparing products to ground based measurements, especially in Greenland (Figure S2c in Supporting Information S1). Consequently, in polar regions, the surface Cloud Radiative Effects (CRE) derived from space-based lidar and space-based radar observations are also more reliable than the ones based on passive radiometers only. We use two sets of surface LWCRE over the GrIS surface: the LWCRE-LIDAR product covers 12 years (2008–2020) and the 2BFLX product covers 5 years (2006–2011). Although these products are not fully independent because they both use CALIPSO Level 1 data, they are different because they do not process it the same way and the 2BFLX algorithm also uses complementary observations (MODIS and CloudSat).

The LWCRE-LIDAR product (Arouf et al., 2022) provides estimates of surface LWCRE from the CALIPSO-GOCCP lidar cloud product. We use this data set at three different resolutions: (a) the monthly gridded LWCRE-LIDAR (2° × 2°) data set is used to examine the surface LWCRE climatology and seasonal cycle over the GrIS, the GrIS west coast and near Summit station (Section 3); (b) the daily gridded LWCRE-LIDAR (1° × 1°) data set is used to build Figure 8 in Section 5; and (c) the LWCRE-LIDAR orbit data set provides the surface LWCRE retrievals at the footprint resolution (330mx90 m) and is used to build Figure 7 (Section 5). Both morning and afternoon orbit data sets are used.

The 2BFLX-LIDAR P1_R04 (hereafter, 2BFLX) product (L'Ecuyer et al., 2008) provides surface LWCRE and surface shortwave Cloud Radiative Effect (SWCRE) estimates derived from CloudSat, CALIPSO and MODIS measurements between 2007 and 2010. We use 2BFLX monthly gridded data at 2.5° × 2.5° resolution to build climatologies of surface cloud radiative effect (Figures 1 and 2).

We also use ground-based measurements of surface LWCRE at the Summit Station (72″N, 38″W) (Miller et al., 2015). Monthly mean values are derived from 30-min surface flux observations at the station. These measurements at Summit Station are used to evaluate the performance of the LWCRE-LIDAR product over Greenland. In order to conduct the comparison, we extract data from the LWCRE-LIDAR monthly gridded data set at the pixel that contains Summit Station.

2.3. Greenland Mass Balance

Space-based gravimetry is used to characterize the spatial variability of Greenland melt. The GRACE data set (Gallagher et al., 2022) provides mass concentration retrievals at a resolution of roughly 100 km × 300 km above Greenland over the period 2001–2023. The resolution is not fine enough to analyze the behavior of a specific glacier, but relevant to get the bigger picture view of how melt is distributed across the surface of Greenland. Data are given in mm of water equivalent. We derive a mass concentration in gigatons based on individual pixel surfaces and water density. This data set is used to build the mass loss map (Figure 1). Mass loss is defined as the difference between the mean mass concentration (in Gt) of 2021 and the mean mass concentration of 2002 for each pixel.

2.4. Low Troposphere Winds

Wind profiles are extracted from the fifth generation European Centre for Medium-Range Weather Forecasts reanalysis (ERA5), that provides daily gridded data at a 1° × 1° resolution between 2008 and 2020 (Hersbach et al., 2020). Only the two horizontal components of winds are considered here. Horizontal wind profiles over the Baffin Sea area (defined in Figure 1) are averaged vertically between the surface and 3 km of altitude, giving what we call hereafter the "lower troposphere wind" over each 1° × 1° pixel.

2.5. Latent Heat Flux and Relative Humidity

Latent heat flux and relative humidity are extracted from ERA5 daily gridded data at a 0.25° × 0.25° resolution between 2008 and 2017 (Hersbach et al., 2020). It provides valuable insights into the moisture origins associated with atmospheric patterns in Baffin Sea (Figure 7). It is important to note that our objective does not encompass the quantitative impact of the moisture intrusion over the GrIS west coast. The scarcity of observational data engenders significant challenges in generating reliable reanalysis data sets for the Arctic region. Uncertainties on air-sea fluxes are specifically high (Boisvert et al., 2015; Chaudhuri et al., 2014), and do not show strong improvements over the new generation for ECMWF reanalysis (C. Wang et al., 2019; W. Wang et al., 2019).

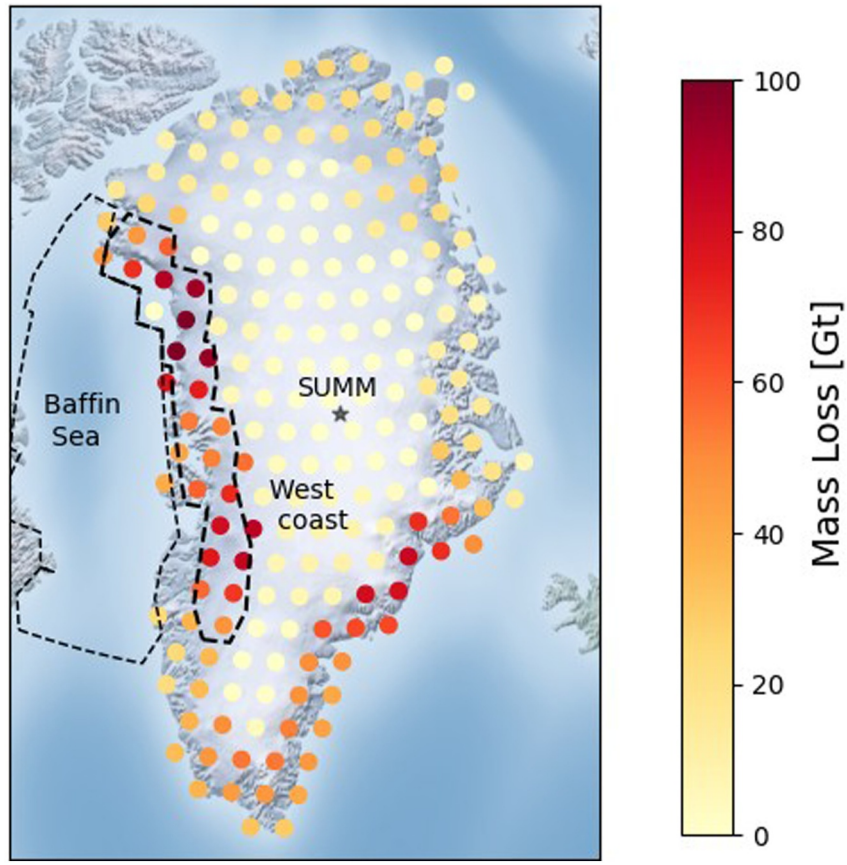

Figure 1. Greenland mass loss derived from GRACE observations, computed as the mean mass of 2002 minus the mean mass of 2021. Similar to (Khan et al., 2015) but over 2002–2021 instead of 2002 and 2014. The Baffin Sea and the Greenland West coast domains are delimited by the black lines. SUMM is the location of the Summit Station.

2.6. Compositing Days With and Without Low Clouds

We identified days "with low clouds over the GrIS west coast" and days "without low clouds over the GrIS west coast." The first step consists of averaging vertical cloud fraction profiles from the CALIPSO-GOCCP daily gridded data set over all the 1° x1° gridboxes contained in the GrIS west coast area (shown in Figure 1). This step gives the mean vertical cloud fraction profile over the GrIS west coast domain for each day between 2008 and 2020. Pixels over the GrIS west coast were already clustered into one single region in Gallagher et al., 2020 for their cloud similarities. The second step consists of averaging each of these profiles between 0.7 and 3.6 km altitude above sea-level (asl), hereafter called the daily low cloud fraction over the GrIS west coast. Finally, days with a daily low cloud fraction over the GrIS west coast above 15% are considered to be those "with low clouds over the GrIS west coast," and days with a daily low cloud fraction over the GrIS west coast below 3% are considered to be those "without low clouds over the GrIS west coast." Based on the distribution (not shown) of daily low cloud fraction values, values below 3% correspond to around 30% of the days and values above 15% correspond to around 30% of days between 2008 and 2020, and therefore days with values between 3% and 15% represent 40% of days between 2008 and 2020.

We compute the mean lower troposphere winds over the Baffin Sea over days "with and without low clouds over the GrIS west coast." Similarly, we compute the mean of the LWCRE-LIDAR daily gridded data set for days "with and without low clouds over the GrIS west coast." We also built the probability density function of surface LWCRE over the GrIS west coast using the LWCRE-LIDAR orbit data set at the footprint scale (330 m × 90 m).

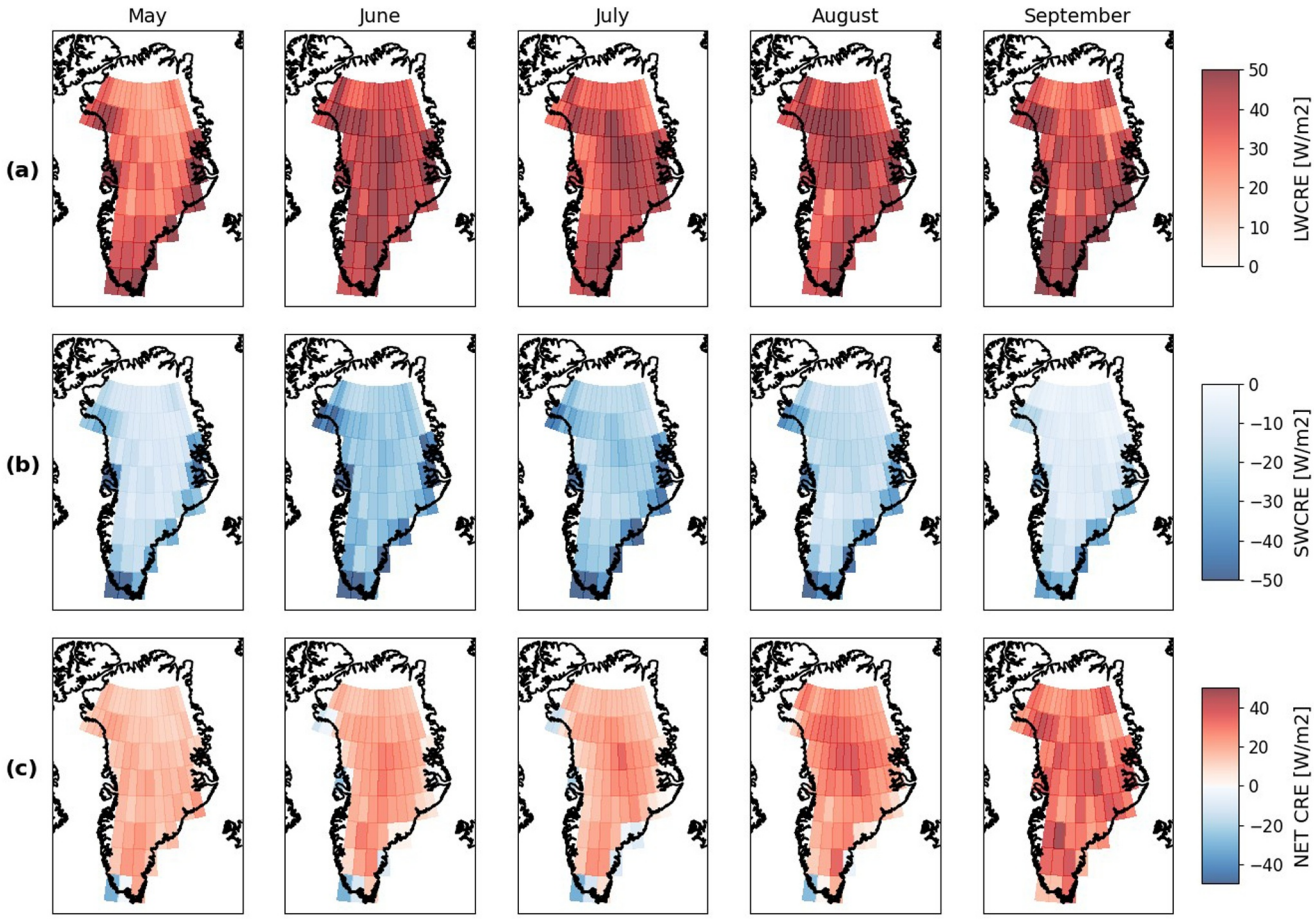

Figure 2. Monthly mean map of (a) LWCRE, (b) SWCRE and (c) the sum of both terms called NET CRE from 2BFLX monthly gridded data set over the period 2007 to 2010.

3. Climatologies

3.1. Mass Loss Context

Over the last two decades, an important amount of the GrIS mass loss happened in narrow bands along the west coast and southeast coast (Figure 1). The mass loss is the result of the balance between the mass accumulated through precipitation and the GrIS melt through multiple mechanisms (See introduction). The spatial variability of mass loss highlighted in Figure 1 can be partly explained by the spatial variability of precipitation. The GrIS west coast, unlike the GrIS southeast coast, does not get as much winter precipitation from the North Atlantic storm track (Gallagher et al., 2022). This suggests that the mass loss of the GrIS west coast is largely driven by the melt processes and motivates us to focus on specific processes that might impact the melting of the GrIS west coast. In this paper, we do not attempt to explain all melt processes in action, but instead focus on one of them: the surface radiative warming produced by low opaque clouds.

Over the rest of this paper the GrIS west coast domain is delimited by the black contour in Figure 1, extending from the Davis Strait (67°N) to the northern most latitude of the Baffin Sea (77°N). The eastern border is defined by the 2,000 m surface elevation contour, approximately corresponding to the limit where melt most often occurs (Karlsson et al., 2021). The Baffin Sea is limited to 67° and 77°N, and surrounded by the Nunavut landmass on the west and the GrIS west coast on the east.

3.2. Surface Cloud Radiative Effect

Here we show the surface LW cloud warming and the surface SW cloud cooling during each month from May through September over the GrIS. Overall, Figure 2 shows that the cloud net radiative effect throughout the entire summer is mainly positive, that is to say that clouds radiatively warm the surface of the GrIS.

In May, the surface LWCRE is lower than for any other summer month, and the SW cooling CRE is particularly important on the GrIS southeast coast. However, the net surface cloud radiative effect remains positive and the clouds radiatively warm the GrIS surface. In June and July, the surface albedo at the edges of the GrIS gets lower and the incoming solar radiation reaches its maximum along the GrIS coasts which results in a maximum surface cloud cooling over the GrIS coasts. But even in these conditions the surface net cloud radiative effect is still slightly positive or close to 0. In September, the surface cloud SW cooling effect is again smaller because of lower sun angles. The higher LWCRE surface warming in September causes a higher net surface cloud warming, specifically on the west coast. Consequently, the surface LWCRE drives the net overall impact of clouds on the GrIS west coast surface radiative budget.

Figure 3a shows the seasonal variability of the GrIS surface LWCRE as derived from two satellite remote sensing products and one set of ground-based measurements. The amplitude and phase of the seasonal cycle of the two satellite products (2BFLX and LWCRE-LIDAR) over the whole GrIS are similar. The mean annual value from 2BFLX is 12 W/m^2 larger compared to the LWCRE-LIDAR product. This difference might be explained by uncertainty of humidity profiles in each product (Arouf et al., 2022; Henderson et al., 2013) and uncertainties in the cloud base height estimation by CALIPSO for LWCRE-LIDAR. However, the LWCRE-LIDAR product is available over a long period of 12 years with daytime and nighttime observations (2008–2020).

To evaluate the LWCRE-LIDAR product over Greenland, we show a comparison with ground-based observations at Summit (for more evaluation see Arouf et al., 2022) as Summit station is the most suitable comparison point due to the absence of comparable data sets within the GrIS west coast. This comparison (Figure 3c) shows similar amplitude and phase of both seasonal cycles, where the satellite LWCRE-LIDAR product mainly underestimates the mean value (−18 W/m^2). The difference primarily arises from the CALIPSO-GOCCP limitation to observe the optically thin ice clouds close to the surface (ice water content <2.5 10^{-3} g/m^3) (Arouf et al., 2022; Lacour et al., 2017), as CALIPSO-GOCCP is used to derive the LWCRE-LIDAR. Lacour et al. (2017) also refers to sampling considerations that might explain biases between ground observations and space-based observations. Even if LWCRE peaks all over summer in central GrIS, the modulation of clouds on the surface radiative budget in this region does not influence melt since annual temperature remains still way below the 0° threshold most of the time (Adolph et al., 2018). As the focus of this study is on the GrIS west coast, Figure 3b shows the seasonal cycle of surface LWCRE over this coastal region. Overall, both over the entire GrIS and the GrIS west coast, summer surface LWCRE values are above the multiyear climatological mean (Figures 3a and 3b), except for July above the GrIS west coast. However, the GrIS west coast experiences a decrease in July and August. As a result, the maximum surface LWCRE over the GrIS west coast happens in September on both LWCRE-LIDAR (33 W/m^2) and 2BFLX (50 W/m^2). It is notable to see that June also experiences a local peak at ∼27 W/m^2 in absolute value of surface LWCRE based on LWCRE-LIDAR, although both data sets agree that this peak is lower than the September peak, and the peak is smaller in the longer data set.

3.3. Vertical Cloud Distribution

Figure 4a highlights the seasonal cycle of the cloud fraction profiles driving the surface LWCRE over the GrIS. Clouds below 4 km above ground level are present from May to September with values of cloud fraction around 14%. Higher clouds, between 4 and 6 km above ground level are persistent over the entire GrIS throughout the year, except for March.

Figure 4b highlights the same cloud properties over the GrIS west coast. Again, high clouds between 4 and 7 km above ground level are persistent all year long except in March. As these clouds emit at lower temperature and have opacity lower than low clouds described later (Figure S1 in Supporting Information S1), these high clouds are likely not critical for understanding drivers of surface LWCRE over the GrIS west coast. The presence of enhanced low clouds over the GrIS west coast between the surface and 3 km above ground level starts in May with maximum fractions around 14%. This feature is intensified in June, but at slightly higher altitude (∼3.5 km asl) with a maximum cloud fraction around 14%. On the contrary to the entire GrIS, low cloud fraction drops in July

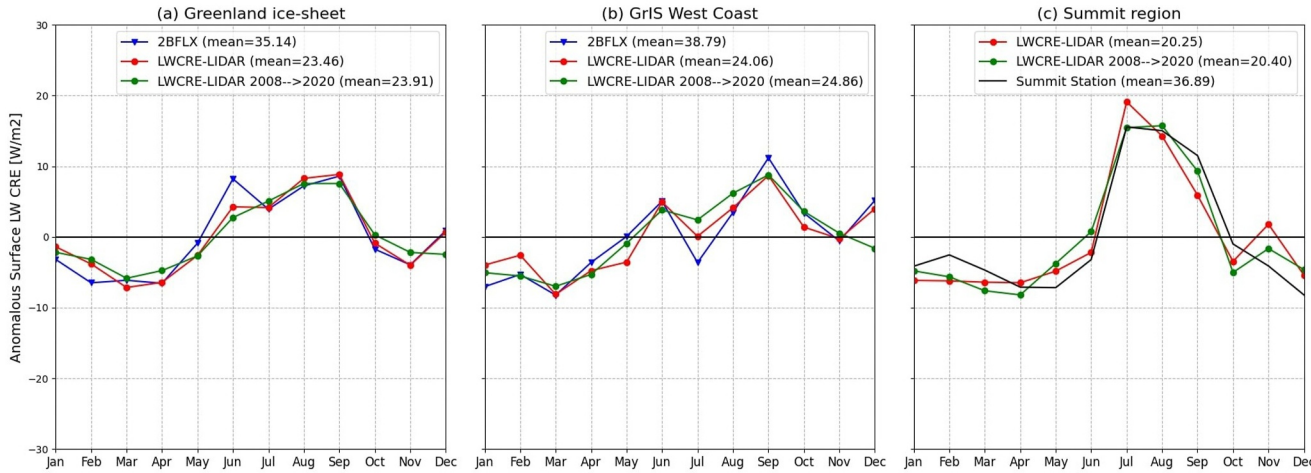

Figure 3. Surface LWCRE seasonal cycle (a) over the Greenland Ice Sheet (GrIS) (2008–2010), (b) over the GrIS west coast (2008–2010), (c) at Summit Station (2011–2015). Time periods correspond to the overlap between different surface LWCRE products. Seasonal cycles are reported as an anomaly with respect to the multiyear climatological mean. Data are provided by LWCRE-LIDAR monthly gridded data set and 2BFLX monthly gridded data set. For additional information, green lines are the surface LWCRE seasonal cycle computed on the entire available period of 2008–2020 of the LWCRE-LIDAR data set.

and August, with maximum values of 10%. Moving from August to September, the presence of low clouds increases again to 14% at 1.2 km above ground level. It is noteworthy to mention that low clouds in September exhibit a comparatively higher opacity when compared to June (Figure S1 in Supporting Information S1).

As the Baffin Sea is the closest body of water to the GrIS west coast and is likely to be a source of moisture and cloudiness for this region, we investigate the same cloud properties over the Baffin Sea. Figure 4c over the Baffin Sea highlights a sharp increase in the cloud fraction below 2 km above ground level from 12% in April to 19% in May. Clouds in the first 200 m persist all through summer. Then, cloud fraction increases again below 2 km above ground level during the fall season. The formation of fall low clouds over the entire Arctic Ocean was explained by Morrison et al. (2018) and occurs consistently in the Baffin Sea based on Figure 4c. The retreat of sea ice in the Baffin Sea during the beginning of June exposes new open water that persists until November. As the lower troposphere temperature decreases from August to September, the coupling between the ice-free ocean and atmosphere gets more and more efficient. The coupling becomes efficient enough during September to lead to an increase in the formation of clouds around 1–2 km in altitude that persists until the Baffin Sea is covered by sea-ice again in December. However, for May, since the Baffin Sea is still ice-covered, the mechanism described by Morrison et al. (2018) does not explain the increase in low cloud presence observed.

By combining Figures 4b and 4c, we show a general correspondence between the fraction of low-level clouds over the GrIS west coast domain and the Baffin Sea, with the most significant difference being in June when there is a particularly high occurrence of clouds below 2 km above ground level over the GrIS west coast with relatively fewer low-level clouds occurring over Baffin Sea.

Overall, the summertime LWCRE increase (Figure 3b) is coincident with increases in the occurrence of low clouds on the GrIS west coast (Figure 4), with the modest decrease of LWCRE in July and August relative to the surrounding months being related to relatively fewer low-level clouds during these months.

4. Origins of Low Clouds Over the Greenland Ice-Sheet West Coast

4.1. Regional Circulation Patterns and Vertical Cloud Distribution

To understand the role of regional atmospheric circulation on the presence of low clouds over the GrIS west coast, we use the Self Organizing Maps (SOM) classification of daily sea level pressure (SLP) anomalies presented by Gallagher et al. (2020). The SOM methodology is an unsupervised machine learning algorithm that classifies daily maps of sea-level pressure anomalies since 1979 into 20 representative maps. Each Figure 5 subpanel plot represents a distinct atmospheric circulation pattern. SOM classification was frequently employed to establish connections between synoptic conditions and localized moisture or cloud transport over Greenland (Mattingly

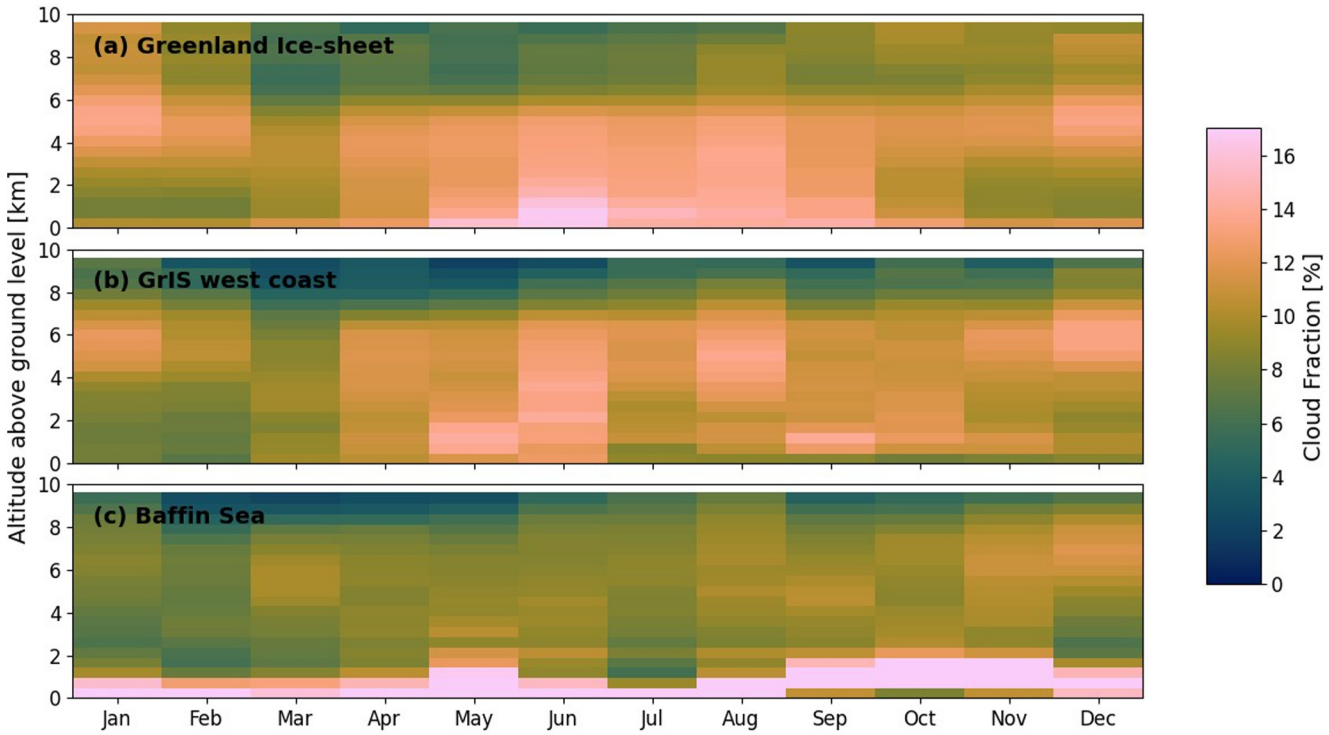

Figure 4. Seasonal cycle of cloud fraction profile (a) over the Greenland Ice Sheet (GrIS) and (b) the GrIS west coast and (c) over the Baffin Sea. The seasonal cycle is obtained from Calipso-GOCCP monthly gridded data over the period 2008–2020. The *Y*-axis represents the altitude of the atmosphere above ground elevation. This latter ranges between 0 and 3.2 km above sea-level for the overall GrIs (plot a) and between 0 and 2 km above sea-level for the GrIS west coast.

et al., 2016; Mioduszewski et al., 2016). Sea-level pressure maps were chosen over other metrics since we investigate processes close to the surface. Each day between 2008 and 2017 is associated with one of the 20 atmospheric circulation patterns shown in Figure 5. Anomalies of vertical cloud fraction profile, surface latent heat flux and vertical relative humidity profile associated with these 20 atmospheric circulation patterns (Figures 6 and 7) are built using every day between 2008 and 2017.

A first look at the histograms of monthly occurrence for each pattern shows that each month of the melt season is associated with a distinct combination of SLP patterns and therefore different atmospheric circulations. Starting in May, patterns D4 and E4, with both a low-pressure system in the North Atlantic Ocean and a weak positive SLP anomaly in the Baffin Sea and over Greenland, represent the main circulation patterns (18%). June, July and August exhibit mainly the occurrence of patterns in the upper part of the SOM characterized by generally lower pressure to the west of Greenland and higher pressure to the east driving wet and warm air masses coming from the North Atlantic Ocean. September shows a unique feature with the nodes of maximum occurrence being in the upper left side of the SOM characterized by the influence of a weak low in the Baffin Sea that is cut off from the primary low-pressure feature that is to the east of Greenland. One potential impact of these patterns would be to slightly pull the Baffin Sea air masses southeastward. Moving to October, patterns that occur most frequently are in the lower part of the SOM. For example, the patterns in B4 and C4 are described by a weak high west of the Baffin Sea and a weak low east of the Baffin Sea. These patterns should slightly pull air masses from the Baffin Sea southward.

Cloud fraction profile anomalies for each circulation pattern over the GrIS west coast, over the Summit region and over the Baffin Sea (See Figure 6) are calculated following the method described in the caption Figure 6. By looking at the cloud fraction profile anomalies over the GrIS west coast for each circulation pattern, we highlight that the A patterns are correlated with positive anomalies of low clouds over the GrIS west coast, as well as a slight positive anomaly in the Baffin Sea. This positive low cloud anomaly is associated with a negative high cloud anomaly for the patterns A3 and A4 and associated with a second positive high cloud anomaly for the patterns A1 and A2 for both the GrIS west coast and the Baffin Sea. Overall, the A patterns are defined by air

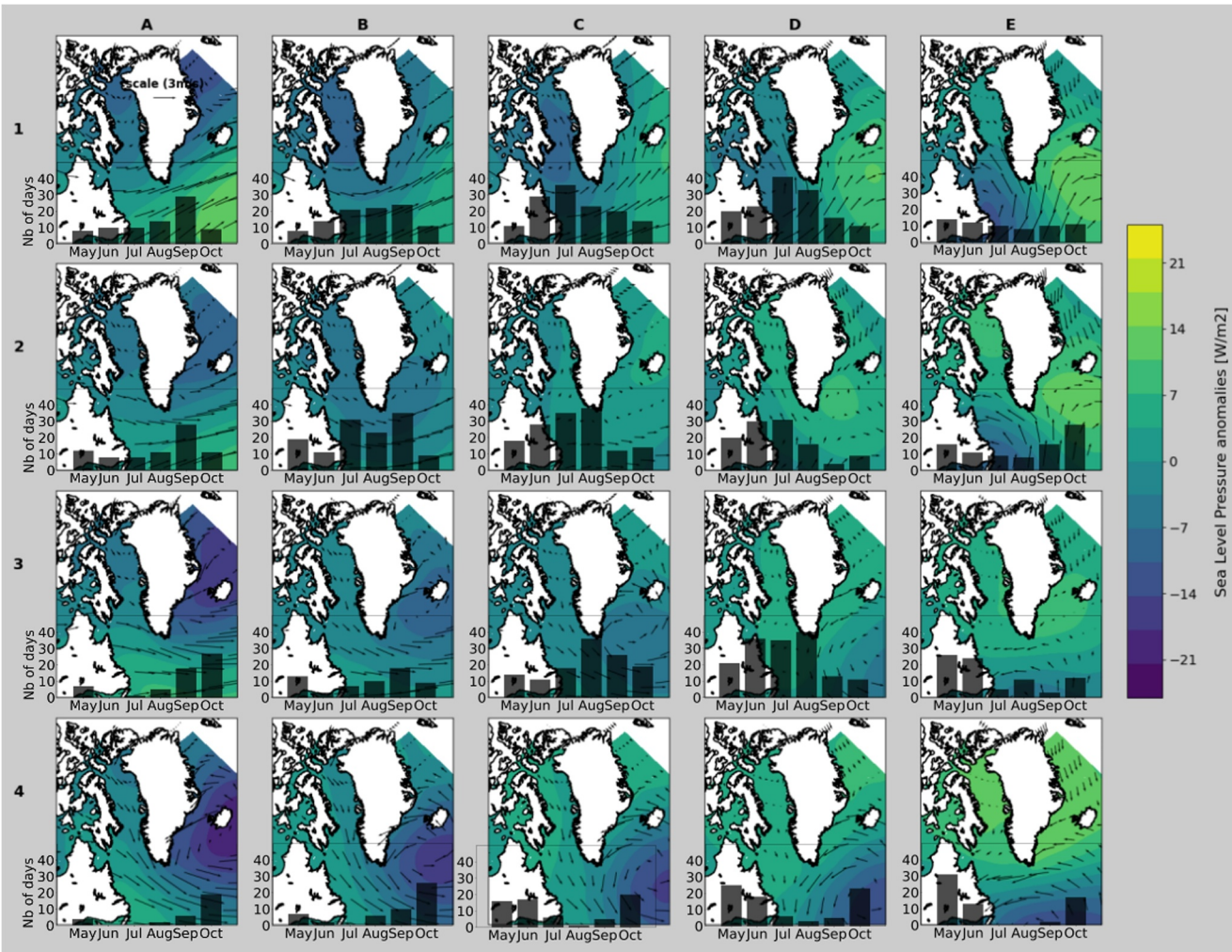

Figure 5. Atmospheric circulation patterns presented by Gallagher et al. (2020) illustrated here with Sea-Level pressure (SLP) anomaly maps and lower troposphere wind maps from ERA5. Daily SLP anomaly maps are computed as the daily SLP maps minus the SLP map averaged over the period 2008 and 2017 for this exact same day of the year. Atmospheric circulation patterns are daily SLP anomaly maps averaged over all the days of a given pattern. Black histograms show the number of days of each pattern for each month between May and October. Histograms are shown only for melt season to facilitate the readability of the figure although it exists for every month.

masses coming from west of Greenland and going through the Baffin Sea before reaching the GrIS west coast. These occur frequently in September and appear to promote the presence of low clouds on the GrIS west coast. Pattern B4 and C4, occurring mainly in October explain the October increase of low clouds in the Baffin Sea observed Figure 4c as the anomaly connected to these patterns is strongly positive below 2 km asl. Although B4 and C4 support the formation of low clouds in the Baffin Sea, air masses are pulled strictly southward. These patterns do not promote the advection of air masses on the GrIS west coast late in fall. The shifting in atmospheric patterns between September and October might explain the decrease of low clouds over the GrIS west coast in October disconnected with the Baffin Sea low cloud variability.

Figure 6 also highlights the importance of patterns B1, C1, D1, E1, and to some extent C2 and D2, to promote positive anomalies in the presence of clouds over the GrIS west coast and over the Summit station region. Thus, low pressure systems, located southwest of Greenland, representative of melt season atmospheric circulation patterns, affect the cloud cover over both coastal regions and the top of the ice-sheet during melt months (consistent with Gallagher et al., 2020). However, these cloud occurrence anomalies typically occur between 4 and 11 km asl. Thus, although these patterns seem to promote clouds over the GrIS west coast, they are not critical for the low cloud fraction over the GrIS west coast.

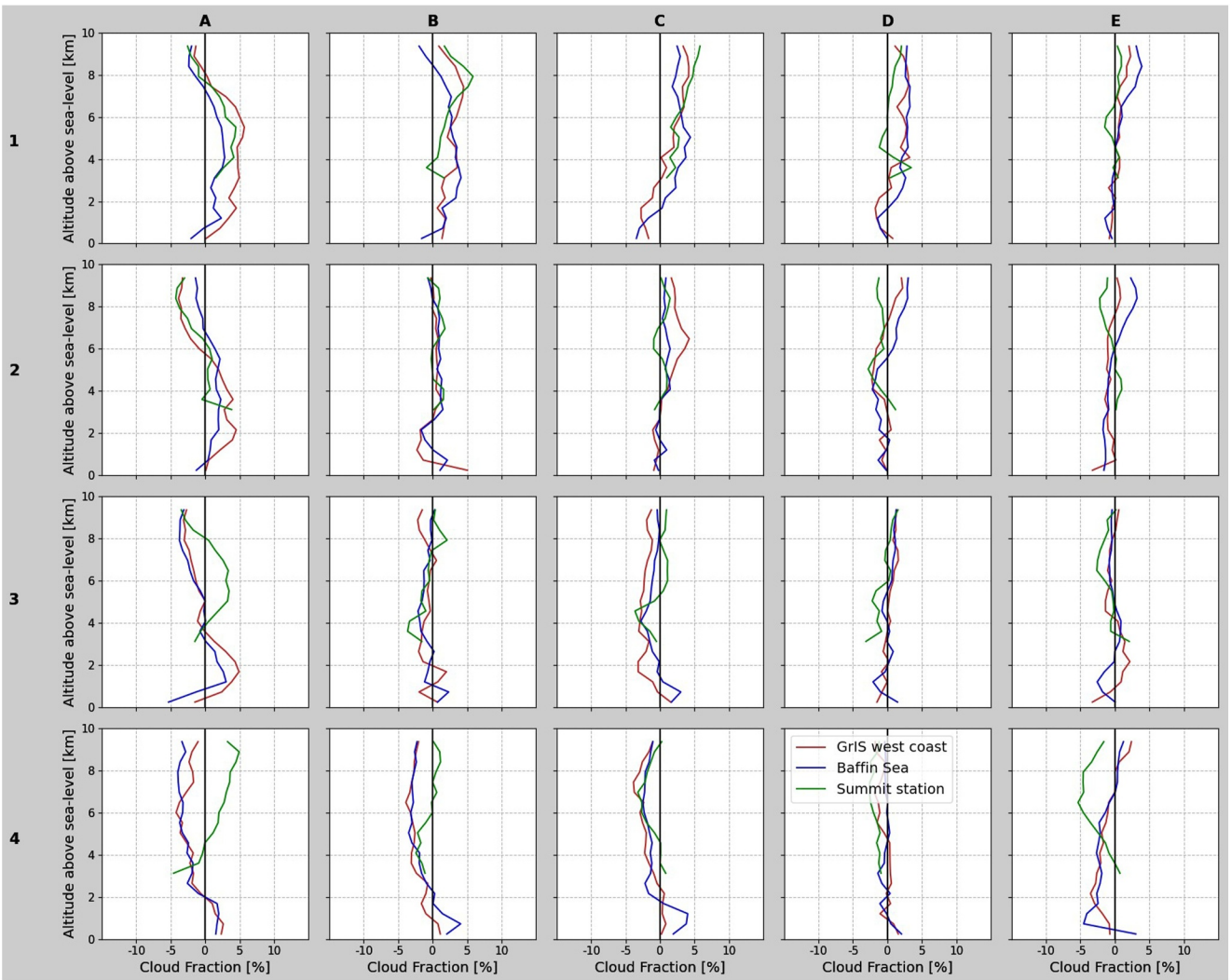

Figure 6. Cloud fraction profile anomalies observed over the Greenland Ice Sheet west coast (red line), the Summit region (green line) and the Baffin Sea (blue line) for each circulation pattern presented Figure 5. For a given circulation pattern, the cloud fraction profile anomaly is the average of the daily cloud fraction anomaly over all the days associated to this given pattern. The daily cloud fraction profile anomaly is the daily cloud fraction profile minus the cloud fraction profile averaged over the period 2008–2017 for this exact same day of the year (moving average over 7 days). Daily cloud fraction profiles are provided by CALIPSO-GOCCP daily gridded (1° × 1°) data set between 2008 and 2017.

4.2. Water Vapor Source

The open ocean and atmosphere coupling in the Baffin Sea might not represent the only contribution of humidity for low cloud formation that leads to low cloud presence associated with polar low circulation (A patterns). There is a need to provide more evidence to demonstrate the role of local water vapor uptake within the Baffin Sea for low cloud formation. Relative humidity profile anomalies over the GrIS west coast (See Figure 7a) and maps of surface latent heat flux anomalies (See Figure 7b) for each circulation pattern are calculated following the method described in the caption Figure 7.

Figure 7a shows that patterns A1, A2 and A3 promote the presence of wet air masses above the GrIS west coast. Maximum positive relative humidity anomalies are captured at 2 km above sea level (asl) for A patterns, matching the altitude of maximum positive anomalies for cloud fraction profiles for the same patterns (Figure 6). Considering the low altitude of maximum relative humidity anomalies, it is likely that air masses going over the Baffin Sea drive a water vapor uptake during melt season over the newly open Baffin Sea water before reaching

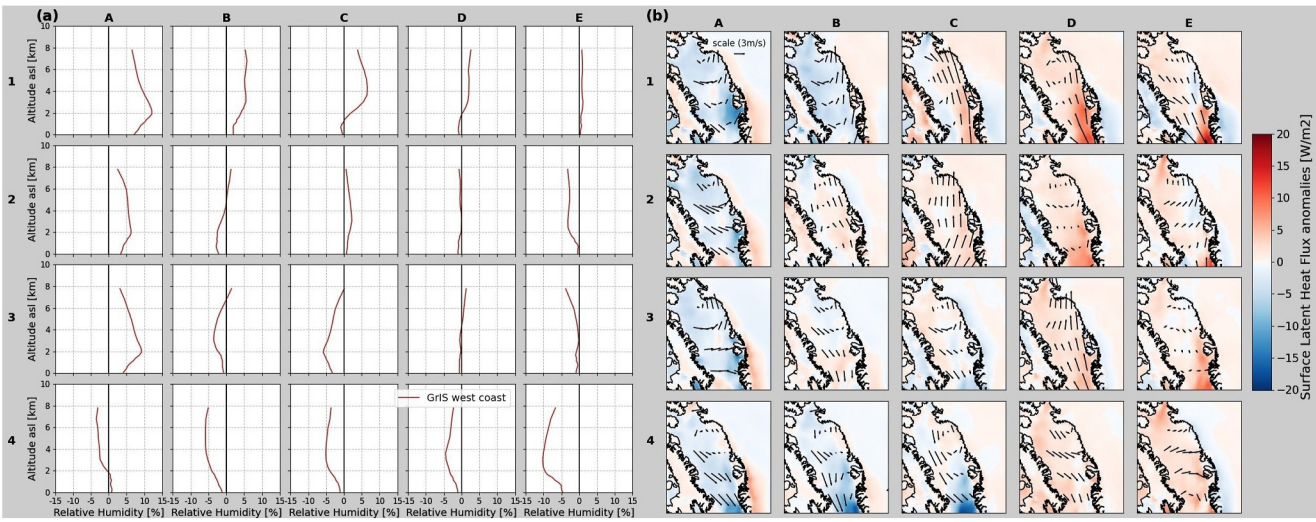

Figure 7. (a) Relative humidity profile anomalies over the Greenland Ice Sheet (GrIS) west coast for each circulation pattern presented Figure 5. For a given circulation pattern, the relative humidity profile anomaly is the average of the daily relative humidity anomaly over all the days associated to this given pattern. The daily relative humidity profile anomaly is the daily relative humidity profile minus the relative humidity profile averaged over the period 2008–2017 for this exact same day of the year. Daily relative humidity profiles are provided by ERA5 daily gridded (0.25° × 0.25°) data set between 2008 and 2017. (b) Same approach with surface latent heat flux provided by ERA5 daily gridded data set (0.25° × 0.25°). Positive anomalies (in red) mean weaker water vapor uptake and negative anomalies (in blue) mean stronger water vapor uptake. Maps focus on the Baffin Sea and the GrIS west coast regions (64–78°N and 44–76°W).

the GrIS west coast. Again, the other row 1 patterns also promote the presence of moisture but at higher altitudes (above 3 km asl).

Figure 7b emphasizes the key role of the Baffin Sea for moistening air masses for days associated with A patterns by looking at surface latent heat flux. Results show that A patterns have some of the strongest negative latent heat anomalies over Baffin Sea, indicating evaporation from the surface into the atmosphere, with the most extreme values close to the southern part of the GrIS west coast region. Thus, the Baffin Sea contributes to lower troposphere moisture content that can then be transported over the GrIS west coast during polar low circulation patterns. Patterns that promote advection of air masses from the North Atlantic (i.e., patterns C1, C2, D1, and D3) are all coincident with weaker surface evaporation in the Baffin Sea.

Overall, our interpretation is that the seasonal ice retreat from April to September in the Baffin Sea allows for more surface evaporation, especially when cold and dry air is often advected from the continental region of Nunavut during September and October (patterns A in September, B4 and C4 in October). The atmosphere moistening in the Baffin Sea leads to low cloud formation that impacts the very localized GrIS west coast when advected by a westerly flow component (patterns A) and do not impact the GrIS west coast when Baffin Sea air masses are strictly advected to the south (B4 and C4 in October).

Nevertheless, we acknowledge the influence of southerly flows on cloud presence over the GrIS west coast primarily during the summer, as Gallagher et al. (2020) showed. Air masses from the south bring pre-existing moist and warm air masses, thereby exhibiting reduced potential for further evaporation upon traversing the relatively cooler Baffin Sea. These air masses have higher buoyancy that might explain the strong positive cloud anomaly of clouds above 5 km asl for these patterns, as they tend to ascend when encountering the colder air masses over the GrIS region. For the specific case of the GrIS west coast, these higher clouds do not appear to control the overall surface cloud radiative warming.

Springtime clouds might be a key process for preconditioning the surface for earlier melt (Cox et al., 2016) by warming the firn toward the melting point. Figure 4 highlights the presence of low clouds in May and June over the Baffin Sea and the GrIS west coast. However, the results presented here in Figures 6 and 7 do not explain the presence of these clouds. None of the atmospheric patterns mainly represented in May show a positive anomaly of low cloud fraction in the Baffin Sea or over the GrIS west coast. The Baffin Sea transitions between sea-ice covered in April to sea-ice free in July. May and June correspond to a period of strong sea ice cover

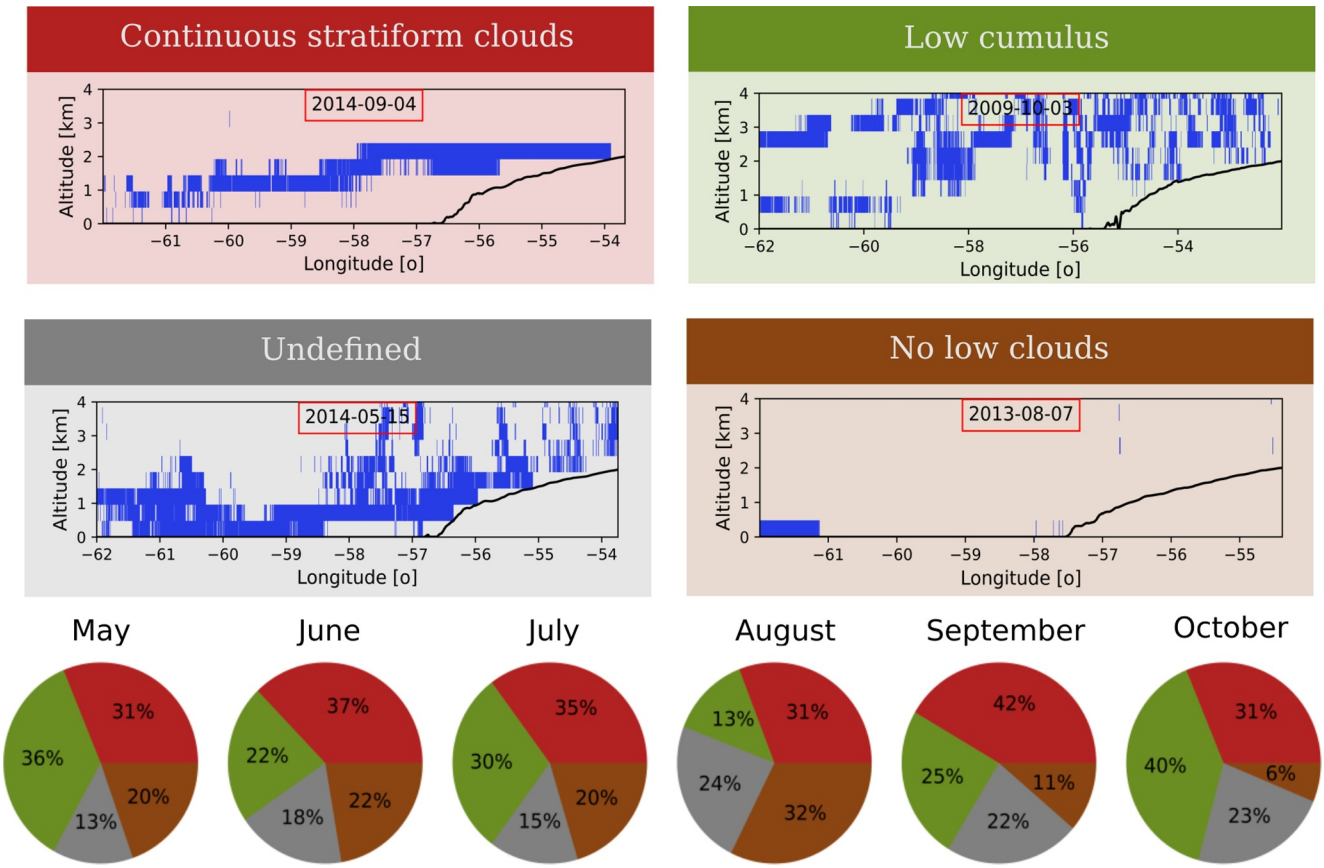

Figure 8. (top) Four categories of cloud types observed across the Baffin Sea and the Greenland Ice Sheet (GrIS) west coast during morning orbits. Blue flag corresponds to CALIPSO-GOCCP cloud mask and the black line corresponds to the GrIS surface. (bottom) Occurrence frequency of each category for months between May and October during days WITH low clouds over the GrIS west coast. "No low clouds" category means that no low clouds were observed in the morning orbit but low clouds have necessarily been observed during the afternoon orbit of the same day as we focus on days WITH low clouds over the GrIS west coast. Cloud observations are provided by the CALIPSO-GOCCP orbit data set between 2008 and 2020.

variability in the Baffin Sea and therefore the coupling between the atmosphere and the ocean that could favor the local formation of low clouds is likely to be much more variable during these months contrarily to September.

4.3. Cloud Continuity From the Baffin Sea to the GrIS West Coast

To further explore the spatial cloud connections for the days with low clouds over the GrIS west coast, we investigate the cloud continuity between the Baffin Sea and the GrIS west coast. For this analysis, we use only the morning orbit of CALIPSO-GOCCP, as morning orbits observe both the Baffin Sea and the GrIS west coast in a single piece of orbit. Visual inspection of every morning orbit allows us to identify strong similarities in cloud structure between the Baffin Sea and the GrIS west coast region. Therefore, orbits are classified into four categories (Figure 8): continuous stratiform clouds, low cumulus clouds, undefined and no low clouds over the GrIS west coast. The latter classification means that no low clouds were observed in the morning orbit over the GrIS west coast but low clouds have necessarily been observed during the afternoon orbit of the same day as we focus on days with low clouds over the GrIS west coast. Undefined classification contains orbits with both low cumulus and stratiform clouds over the GrIS west coast and also orbits with non-continuous stratocumulus between the Baffin Sea and the GrIS west coast. We differentiate cumulus and stratiform clouds by their vertical variability and their horizontal extent. Cumulus are described by high vertical variability and low horizontal extent whereas stratiform clouds are described by lower vertical variability and higher horizontal extent (Cesana et al., 2019). Every piece of morning orbit and their classification are available in Figure S3 in Supporting Information S1.

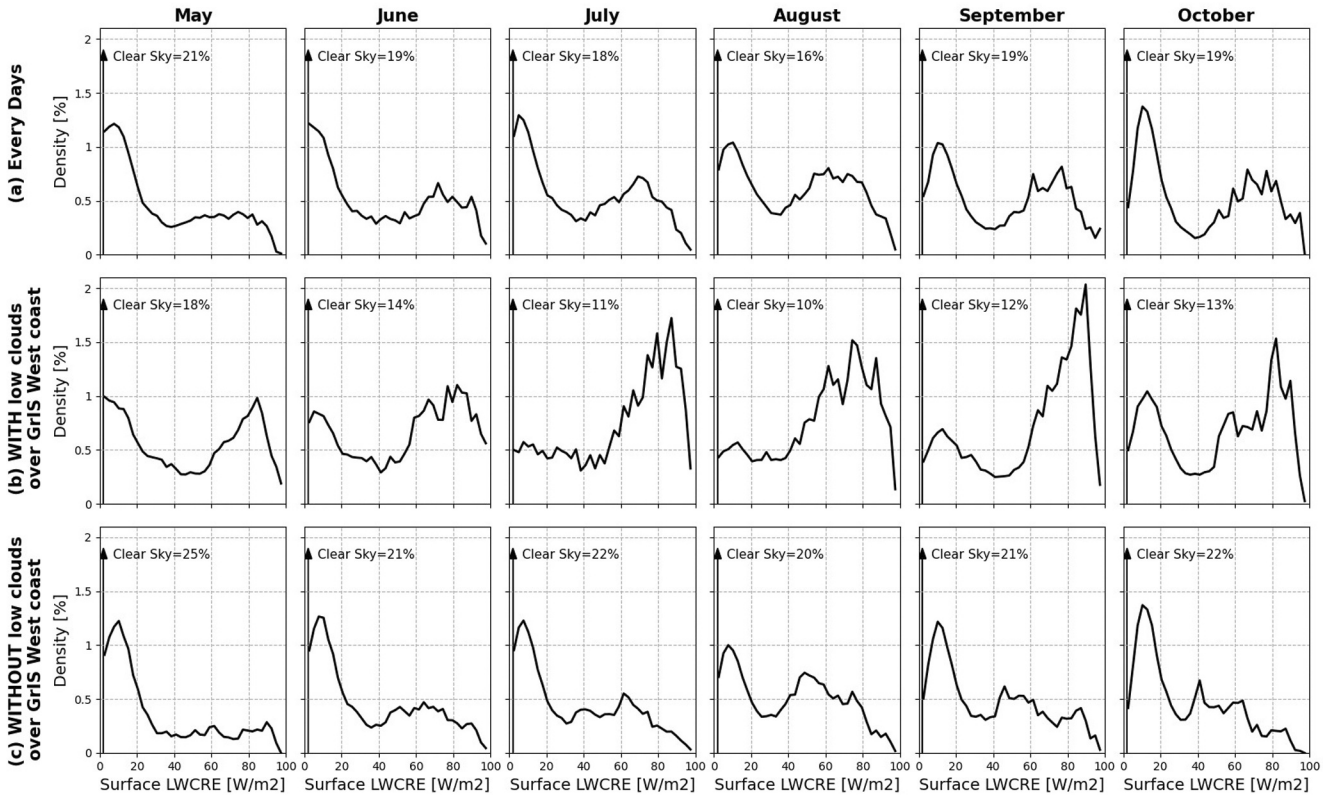

Figure 9. Probability Density Functions (PDF) of Greenland Ice Sheet (GrIS) west coast surface LWCRE (a) for all day, (b) for days WITH and (c) for days WITHOUT low clouds over the GrIS west coast. PDF are built using the LWCRE-LIDAR at footprint scale (330 m × 90 m) using orbit data set over the period 2008–2020. First Surface LWCRE box density (between 0 and 2.5 W/m^2) corresponding to clear-sky (CS) scenes is highlighted in the legend as it dominates by far the PDF.

Between June and September, the analysis of cloud classification distributions reveals that continuous stratiform clouds between the Baffin Sea and the GrIS west coast prevail (36% in average). However, it is worth noting that in August, the "undefined" classification assumes significance, accounting for 32% of observations. This suggests a prevalent coexistence of cumulus and stratiform clouds during this period. September circulation west of Greenland is predominantly driven by a polar low type of circulation leading to southeastward wind in the Baffin Sea (Figure 5), and the exposed open water in Baffin Sea at this time of year can serve as a source of moisture. Thus, it stands to reason that September low clouds over the GrIS west coast predominantly originate from the Baffin Sea region. Indeed, the continuous stratiform clouds linking these two domains are observed 42% of the time during this month, more often than in any other month.

May and October stand as months dominated by low cumulus clouds over the GrIS west coast (respectively 36% and 40% of orbits). Again, variability in May of sea ice coverage in the Baffin Sea mitigates the formation of stratiform clouds in the Baffin Sea and might explain this difference. The findings for October corroborate our earlier conclusion regarding the isolation of the GrIS west coast from the Baffin Sea due to the recurrent occurrence of patterns B4 and C4 during this month although stratiform clouds are forming in the Baffin Sea.

5. Radiative Impact of Low Cloud Over the GrIS West Coast

To understand the linkage between the presence of low clouds over the GrIS west coast and higher cloud surface warming in this region (Figure 3), we investigate the cloud surface warming effect at a footprint scale (330 m × 90 m) of the LWCRE-LIDAR (Figure 9) over the GrIS west coast. Considering every day of each melt season month (Figure 9a), we highlight a trimodal behavior of surface cloud warming, with the first mode at 0 W/m^2, the second below 20 W/m^2 and the third one above 60 W/m^2. The first mode corresponds to clear-sky profiles and largely dominates every Probability Density Functions (PDF) presented here. This peak is not part of the analysis as we study the role of clouds on the surface radiative budget. The second mode corresponds to weak

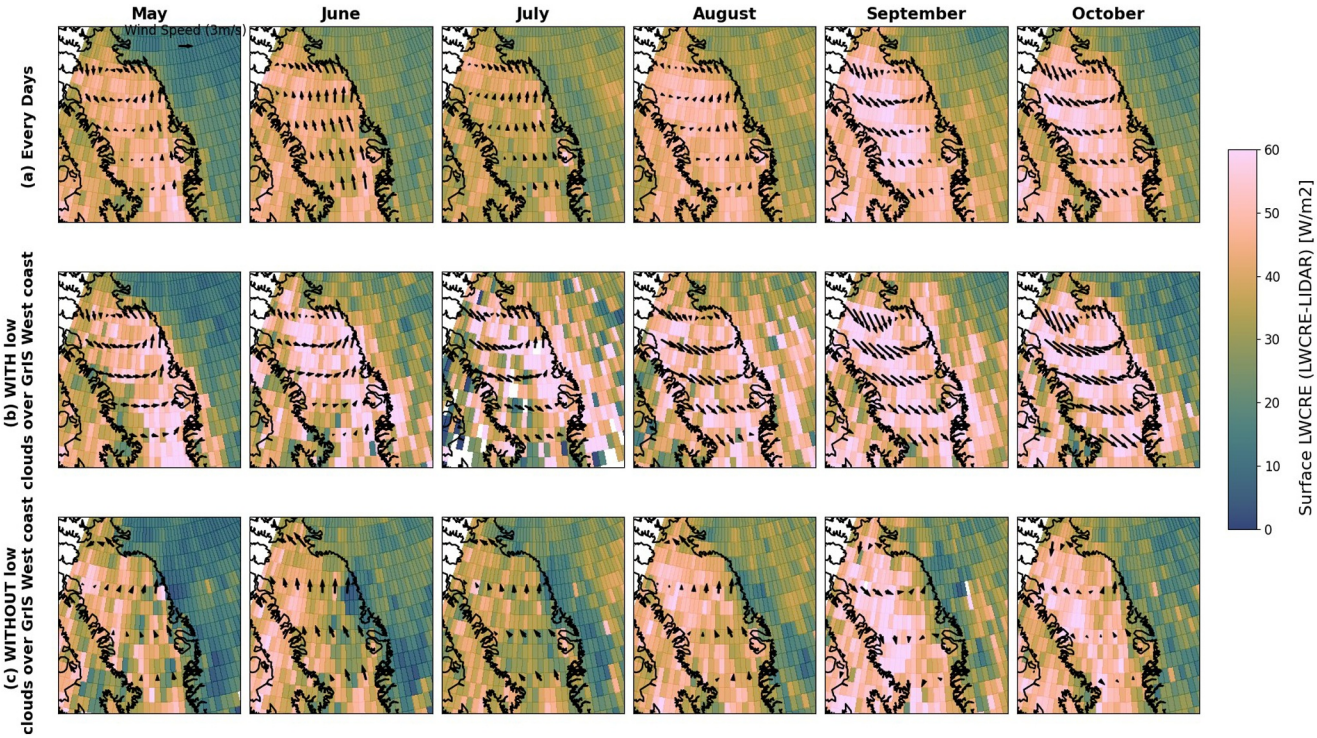

Figure 10. Maps of mean Surface LWCRE in color and lower troposphere wind in black arrows for (a) all day, (b) days WITH, and (c) days WITHOUT low clouds over the Greenland Ice Sheet (GrIS) west coast. The surface LW CRE is provided by LWCRE-LIDAR daily gridded data set and the lower troposphere winds by the ERA5 daily gridded data set between 2008 and 2017. Maps focus on the Baffin Sea and the GrIS west coast regions (64–78°N and 44–76°W).

warming of the surface because there are optically thin clouds. The third peak corresponds to the highest surface LWCRE retrieved from CALIPSO-GOCCP observations (Arouf et al., 2022), and occurs when the cloud is optically thick. PDF built for days with low clouds over the GrIS west coast only (Figure 9b) are dominated by this third mode around 60 W/m^2, yet still have some occurrence of the weaker warming mode, which is likely due to optically thin low clouds composed primarily of ice. Although we isolated days with low clouds over the GrIS west coast, some clear-sky gaps within clouds still exist due to the cloud horizontal variability and explains the existence of a clear-sky peak here (see orbit examples Figure S3 in Supporting Information S1). On the other hand, distributions built for days without low clouds over the GrIS west coast (Figure 9c) are dominated by the first peak around 20 W/m^2, with still some occurrence of the mode with more warming due to optically thick clouds that occur at higher altitudes. Generally, there are far fewer cases of the most extremely positive LW CRE, which indicates that these warming conditions are strongly linked with the occurrence of the low clouds.

Figure 10 summarizes many of the prior conclusions into one single figure. Figure 10a shows that from May to August, on average over all conditions, the Baffin Sea is dominated by northward lower troposphere wind, consistent with the patterns shown in Figure 5. September and October feature a polar low type of circulation characteristic of the A-patterns in the SOM analysis.

By examining these results for cases with and without low clouds over the GrIS west coast, it becomes clear that the Baffin Sea polar low pattern is present to some degree in all months when low clouds are present over the GrIS west coast (Figure 10b). This "with low cloud" pattern is particularly strong in September and October with increased winds in those months. Moreover, days with low clouds over the GrIS west coast typically correspond with much higher surface LWCRE both in the Baffin Sea and the GrIS west coast. The continuity of cloud surface warming between the Baffin Sea and the GrIS west coast during these periods is notable, consistent with observations given in Figure 8. Cloud surface warming for July days with low clouds over the GrIS west coast is high, but fewer occurrence of days with low clouds compared to September help to explain why July cloud surface warming is not as high as September.

Looking at days without low clouds over the GrIS west coast (Figure 10c), from May to August, the Baffin Sea is dominated by northward wind that does not strongly promote the presence of low clouds over the GrIS west coast nor the Baffin Sea. Consequently, the surface cloud warming on the GrIS west coast is significantly lower during these days.

6. Discussion and Conclusion

This study assesses the presence of low clouds over the GrIS west coast during the melt season and examines the origin of these clouds and their influence on the surface radiative warming. First, it is shown that the GrIS west coast has contributed 1,000 Gt of the 4,488 Gt GrIS mass loss between 2002 and 2021 (Figure 1), making it a hotspot for GrIS mass loss. One of the numerous processes that lead to surface melt is warming due to the surface radiative effect of clouds (Figure 2). A broad peak of surface cloud radiative warming occurs on the GrIS west coast during the summer and fall (Figure 3), with some month-to-month variability. Looking at seasonal cloud properties, Figure 4b highlights that the summer warming increase and monthly variations are related to variability in the presence of low clouds over the GrIS west coast as well as over the Baffin Sea. For example, the cloud warming effect during July and August over the GrIS west coast region is modestly less than elsewhere over the ice sheet, compared to other months, as a result of relatively less frequent low clouds over the west coast region during these months. Conversely, September experiences a peak of surface LWCRE over the GrIS west coast as a result of relatively more frequent low clouds. In September, the origin of low clouds over the GrIS west coast was found to be related to polar low circulation patterns in Baffin Sea (Figures 5 and 6). These patterns, shown to occur most strongly in September, result in west-to-east winds over the Baffin Sea. Such transport has been shown to uptake moisture over the seasonally open water in Baffin Sea and contribute to the advection of moist air and clouds from Baffin Sea over the west coast of the GrIS (Figures 7a and 7b). Moving to the processes for low cloud formation (Figure 8), from June to September, cloud typology over the GrIS west coast is dominated by continuous stratiform clouds between the Baffin Sea and the GrIS west coast (36% of CALIPSO morning orbits), and especially in September when continuous stratiform clouds between the Baffin Sea and the GrIS west coast represent 44% of the CALIPSO morning orbits. Examining the impact of these low opaque clouds over the GrIS surface, we found that the monthly mean cloud surface warming increase of +10 W/m^2 in September (compared to July-August) can be attributed to days with low clouds over the GrIS west coast (Figure 9). Indeed, days where low clouds are present on the GrIS west coast result in a distinct mode of surface LWCRE around 60–80 W/m^2.

Considering all of these points, it is reasonable to conclude that the seasonal retreat of sea ice in Baffin Sea and the common atmospheric circulation patterns found there contribute to enhanced summertime cloud formation in the area and enhanced transport of these cloudy airmasses to the western GrIS where they impart significant warming on the surface.

The presence of stratiform liquid-containing clouds on the GrIS west coast with a strong warming effect at the surface raises several important issues to address in future studies.

- The decline of Arctic sea ice extent is predicted to continue, and might result in September ice-free conditions before 2050, according to most of the CMIP6 models (Notz & Community, 2020). The seasonality of the melt is also modified, as shown by Stroeve and Notz (2018), which would tend to keep the ocean sea ice free for a longer period. Even if processes that lead to stratocumulus cloud formation are not fully understood, their link with sea ice retreat associated with strong local ocean/atmosphere coupling seems to be clear (Morrison et al., 2018). As a result, it is yet to be seen if the further decline of sea ice will lead to an increase in the number of low clouds over the Baffin Bay in a warmer future, independent of large scale processes, and therefore increase the number of days with low clouds transported from Baffin Sea over the GrIS west coast leading to an increase of surface radiative warming over the GrIS west coast.
- One previous paper has highlighted the role of clouds in preventing daytime melted ice from refreezing during nighttime due to continued warming at night, thus increasing surface runoff (Van Tricht et al., 2016). As shown in Figure 8, early morning CALIPSO (4–6 a.m. LST) observations capture low clouds over the GrIS west coast in 89% of the September cases. Our analyses thus suggest that the potential effect of days with low clouds over the GrIS west coast on the surface mass balance might be even more important than simply contributing to melt itself. Since these processes of melt and potential refreeze play out over daily cycles, it is important for future studies to examine the diurnal occurrence and impacts of low clouds over the GrIS west coast.

Data Availability Statement

GRACE Mass Variability Time Series were obtained from NASA's GSFC GRACE mascon solutions are included in Gallagher et al. (2022). The GOCCP v3.2 products are included in Chepfer et al. (2010). The LWCRE–LIDAR–Ed1 is available for the 2008–2020 time period at https://doi.org/10.14768/70d5f4b5-e740-4d4c-b1ec-f6459f7e5563 for the monthly gridded data set (Arouf et al., 2022), and at https://doi.org/10.14768/d4de28c3-0912-4244-8c2b-6fe259eb863c for the data set along orbit track. The 2BFLX monthly data set for the 2007−2010 time period is included in Henderson et al. (2013). The ERA5 reanalysis data is publicly available via the Climate Data Store (Hersbach et al., 2020).

Acknowledgments
We thank NASA/CNES for the CALIPSO level-1 data and the mesocenter ESPRI/IPSL for the computational resources. We recognize the support of CNES, who supported the development of the CALIPSO-GOCCP product through EECLAT project. MG and MDS were supported by the National Science Foundation (OPP-2137091) and the National Oceanic and Atmospheric Administration Physical Science Laboratory via cooperative agreement NA22OAR4320151. Constructive comments from two anonymous reviewers greatly helped to improve the manuscript.

References

Adolph, A. C., Albert, M. R., & Hall, D. K. (2018). Near-surface temperature inversion during summer at Summit, Greenland, and its relation to MODIS-derived surface temperatures. *The Cryosphere*, *12*(3), 907–920. https://doi.org/10.5194/tc-12-907-2018

Arouf, A., Chepfer, H., Vaillant de Guélis, T., Chiriaco, M., Shupe, M. D., Guzman, R., et al. (2022). The surface longwave cloud radiative effect derived from space lidar observations. *Atmospheric Measurement Techniques*, *15*(12), 3893–3923. https://doi.org/10.5194/amt-15-3893-2022

Bamber, J. L., Griggs, J. A., Hurkmans, R. T. W. L., Dowdeswell, J. A., Gogineni, S. P., Howat, I., et al. (2013). A new bed elevation dataset for Greenland. *The Cryosphere*, *7*(2), 499–510. https://doi.org/10.5194/tc-7-499-2013

Bennartz, R., Shupe, M. D., Turner, D. D., Walden, V. P., Steffen, K., Cox, C. J., et al. (2013). July 2012 Greenland melt extent enhanced by low-level liquid clouds. *Nature*, *496*(7443), 83–86. https://doi.org/10.1038/nature12002

Boisvert, L. N., Wu, D. L., Vihma, T., & Susskind, J. (2015). Verification of air/surface humidity differences from AIRS and ERA-Interim in support of turbulent flux estimation in the Arctic. *Journal of Geophysical Research: Atmospheres*, *120*(3), 945–963. https://doi.org/10.1002/2014JD021666

Cesana, G., & Chepfer, H. (2013). Evaluation of the cloud thermodynamic phase in a climate model using CALIPSO-GOCCP. *Journal of Geophysical Research: Atmospheres*, *118*(14), 7922–7937. https://doi.org/10.1002/jgrd.50376

Cesana, G., Del Genio, A. D., & Chepfer, H. (2019). The cumulus and stratocumulus CloudSat-CALIPSO dataset (CASCCAD). *Earth System Science Data*, *11*(4), 1745–1764. https://doi.org/10.5194/essd-11-1745-2019

Cesana, G., Kay, J. E., Chepfer, H., English, J. M., & De Boer, G. (2012). Ubiquitous low-level liquid-containing Arctic clouds: New observations and climate model constraints from CALIPSO-GOCCP. *Geophysical Research Letters*, *39*(20), L20804. https://doi.org/10.1029/2012GL053385

Chaudhuri, A. H., Ponte, R. M., & Nguyen, A. T. (2014). A comparison of atmospheric reanalysis products for the Arctic Ocean and implications for uncertainties in air–sea fluxes. *Journal of Climate*, *27*(14), 5411–5421. https://doi.org/10.1175/JCLI-D-13-00424.1

Chepfer, H., Bony, S., Winker, D., Cesana, G., Dufresne, J. L., Minnis, P., et al. (2010). The GCM-oriented calipso cloud product (CALIPSO-GOCCP). *Journal of Geophysical Research*, *115*(D4), D00H16. https://doi.org/10.1029/2009JD012251

Cox, C. J., Uttal, T., Long, C. N., Shupe, M. D., Stone, R. S., & Starkweather, S. (2016). The role of springtime Arctic clouds in determining autumn sea ice extent. *Journal of Climate*, *29*(18), 6581–6596. https://doi.org/10.1175/JCLI-D-16-0136.1

Enderlin, E. M., Howat, I. M., Jeong, S., Noh, M. J., Van Angelen, J. H., & Van Den Broeke, M. R. (2014). An improved mass budget for the Greenland ice sheet. *Geophysical Research Letters*, *41*(3), 866–872. https://doi.org/10.1002/2013GL059010

Gallagher, M. R., Chepfer, H., Shupe, M. D., & Guzman, R. (2020). Warm temperature extremes across Greenland connected to clouds. *Geophysical Research Letters*, *47*(9), e2019GL086059. https://doi.org/10.1029/2019GL086059

Gallagher, M. R., Shupe, M. D., Chepfer, H., & L'Ecuyer, T. (2022). Relating snowfall observations to Greenland ice sheet mass changes: An atmospheric circulation perspective. *The Cryosphere*, *16*(2), 435–450. https://doi.org/10.5194/tc-16-435-2022

Guzman, R., Chepfer, H., Noel, V., Vaillant de Guélis, T., Kay, J. E., Raberanto, P., et al. (2017). Direct atmosphere opacity observations from CALIPSO provide new constraints on cloud-radiation interactions. *Journal of Geophysical Research: Atmospheres*, *122*(2), 1066–1085. https://doi.org/10.1002/2016JD025946

Henderson, D. S., L'ecuyer, T., Stephens, G., Partain, P., & Sekiguchi, M. (2013). A multisensor perspective on the radiative impacts of clouds and aerosols. *Journal of Applied Meteorology and Climatology*, *52*(4), 853–871. https://doi.org/10.1175/JAMC-D-12-025.1

Hersbach, H., Bell, B., Berrisford, P., Hirahara, S., Horányi, A., Muñoz-Sabater, J., et al. (2020). The ERA5 global reanalysis. *Quarterly Journal of the Royal Meteorological Society*, *146*(730), 1999–2049. https://doi.org/10.1002/qj.3803

Hofer, S., Tedstone, A. J., Fettweis, X., & Bamber, J. L. (2017). Decreasing cloud cover drives the recent mass loss on the Greenland Ice Sheet. *Science Advances*, *3*(6), e1700584. https://doi.org/10.1126/sciadv.1700584

Karlsson, N. B., Solgaard, A. M., Mankoff, K. D., Gillet-Chaulet, F., MacGregor, J. A., Box, J. E., et al. (2021). A first constraint on basal melt-water production of the Greenland ice sheet. *Nature Communications*, *12*(1), 3461. https://doi.org/10.1038/s41467-021-23739-z

Kay, J. E., L'Ecuyer, T., Gettelman, A., Stephens, G., & O'Dell, C. (2008). The contribution of cloud and radiation anomalies to the 2007 Arctic sea ice extent minimum. *Geophysical Research Letters*, *35*(8), L08503. https://doi.org/10.1029/2008GL033451

Khan, S. A., Aschwanden, A., Bjørk, A. A., Wahr, J., Kjeldsen, K. K., & Kjaer, K. H. (2015). Greenland ice sheet mass balance: A review. *Reports on Progress in Physics*, *78*(4), 046801. https://doi.org/10.1088/0034-4885/78/4/046801

Lacour, A., Chepfer, H., Shupe, M. D., Miller, N. B., Noel, V., Kay, J., et al. (2017). Greenland clouds observed in CALIPSO-GOCCP: Comparison with ground-based summit observations. *Journal of Climate*, *30*(15), 6065–6083. https://doi.org/10.1175/JCLI-D-16-0552.1

L'Ecuyer, T. S., Wood, N. B., Haladay, T., Stephens, G. L., & Stackhouse, P. W., Jr. (2008). Impact of clouds on atmospheric heating based on the R04 CloudSat fluxes and heating rates data set. *Journal of Geophysical Research*, *113*(D8), D00A15. https://doi.org/10.1029/2008JD009951

Li, X., Krueger, S. K., Strong, C., Mace, G. G., & Benson, S. (2020). Midwinter Arctic leads form and dissipate low clouds. *Nature Communications*, *11*(1), 206. https://doi.org/10.1038/s41467-019-14074-5

Mattingly, K. S., Ramseyer, C. A., Rosen, J. J., Mote, T. L., & Muthyala, R. (2016). Increasing water vapor transport to the Greenland Ice Sheet revealed using self-organizing maps. *Geophysical Research Letters*, *43*(17), 9250–9258. https://doi.org/10.1002/2016GL070424

Miller, N. B., Shupe, M. D., Cox, C. J., Walden, V. P., Turner, D. D., & Steffen, K. (2015). Cloud radiative forcing at Summit, Greenland. *Journal of Climate*, *28*(15), 6267–6280. https://doi.org/10.1175/JCLI-D-15-0076.1

Mioduszewski, J. R., Rennermalm, A. K., Hammann, A., Tedesco, M., Noble, E. U., Stroeve, J. C., & Mote, T. L. (2016). Atmospheric drivers of Greenland surface melt revealed by self-organizing maps. *Journal of Geophysical Research: Atmospheres*, *121*(10), 5095–5114. https://doi.org/10.1002/2015JD024550

Morrison, A. L., Kay, J. E., Chepfer, H., Guzman, R., & Yettella, V. (2018). Isolating the liquid cloud response to recent Arctic sea ice variability using spaceborne lidar observations. *Journal of Geophysical Research: Atmospheres*, *123*(1), 473–490. https://doi.org/10.1002/2017JD027248

Nghiem, S. V., Hall, D. K., Mote, T. L., Tedesco, M., Albert, M. R., Keegan, K., et al. (2012). The extreme melt across the Greenland ice sheet in 2012. *Geophysical Research Letters*, *39*(20), L20502. https://doi.org/10.1029/2012GL053611

Notz, D., & Community, S. I. M. I. P. (2020). Arctic sea ice in CMIP6. *Geophysical Research Letters*, *47*(10), e2019GL086749. https://doi.org/10.1029/2019GL086749

Shupe, M. D., & Intrieri, J. M. (2004). Cloud radiative forcing of the Arctic surface: The influence of cloud properties, surface albedo, and solar zenith angle. *Journal of Climate*, *17*(3), 616–628. https://doi.org/10.1175/1520-0442(2004)017<0616:CRFOTA>2.0.CO;2

Stroeve, J., & Notz, D. (2018). Changing state of Arctic sea ice across all seasons. *Environmental Research Letters*, *13*(10), 103001. https://doi.org/10.1088/1748-9326/aade56

Tedesco, M., & Fettweis, X. (2020). Unprecedented atmospheric conditions (1948–2019) drive the 2019 exceptional melting season over the Greenland ice sheet. *The Cryosphere*, *14*(4), 1209–1223. https://doi.org/10.5194/tc-14-1209-2020

Van den Broeke, M. R., Enderlin, E. M., Howat, I. M., Kuipers Munneke, P., Noël, B. P., Van De Berg, W. J., et al. (2016). On the recent contribution of the Greenland ice sheet to sea level change. *The Cryosphere*, *10*(5), 1933–1946. https://doi.org/10.5194/tc-10-1933-2016

Van Tricht, K., Lhermitte, S., Lenaerts, J. T., Gorodetskaya, I. V., L'Ecuyer, T. S., Noël, B., et al. (2016). Clouds enhance Greenland ice sheet meltwater runoff. *Nature Communications*, *7*(1), 10266. https://doi.org/10.1038/ncomms10266

Wang, C., Graham, R. M., Wang, K., Gerland, S., & Granskog, M. A. (2019). Comparison of ERA5 and ERA-Interim near-surface air temperature, snowfall and precipitation over Arctic sea ice: Effects on sea ice thermodynamics and evolution. *The Cryosphere*, *13*(6), 1661–1679. https://doi.org/10.5194/tc-13-1661-2019

Wang, W., Zender, C. S., van As, D., & Miller, N. B. (2019). Spatial distribution of melt season cloud radiative effects over Greenland: Evaluating satellite observations, reanalyses, and model simulations against in situ measurements. *Journal of Geophysical Research: Atmospheres*, *124*(1), 57–71. https://doi.org/10.1029/2018JD028919

References From the Supporting Information

Kato, S., Rose, F. G., Rutan, D. A., Thorsen, T. J., Loeb, N. G., Doelling, D. R., et al. (2018). Surface irradiances of edition 4.0 clouds and the earth's radiant energy system (CERES) energy balanced and filled (EBAF) data product. *Journal of Climate*, *31*(11), 4501–4527. https://doi.org/10.1175/JCLI-D-17-0523.1